

## Simulated Weathering Tests of Photocatalytic Paint Containing LaFeO<sub>3</sub>

Elena de la Fuente García, Veronica Carrara, Francesca Fontana, Isabella Natali Sora\*

Università di Bergamo, Dipartimento di Ingegneria e Scienze Applicate, Viale Marconi 5, 24044 Dalmine BG, Italy  
[isabella.natali-sora@unibg.it](mailto:isabella.natali-sora@unibg.it)

The effects of simulated weathering tests on water paints based upon a silicate binder, containing a LaFeO<sub>3</sub> photocatalyst, were investigated by measuring their self-cleaning performances. Paint samples were exposed to accelerated ageing tests using a climatic chamber, which simulated weathering effects such as UV radiation, rainwater and conspicuous temperature and humidity variations. Samples were subsequently stained by Procion Red PX4B dye and the color degradation of the taint onto the solid phase was followed through UV–vis diffuse reflectance spectra (DRS). The dye discoloration percentage after 360 h visible light irradiation was 78 % for not weathered samples, and 67 % for weathered ones.

### 1. Introduction

The effects of soiling on outdoor surfaces of buildings are well-known. Among the advanced protecting processes, coating with photocatalytic paint seems a very promising approach toward effective self-cleaning of the building facades. The photocatalytic process appears to be convenient and green in comparison with the traditional maintenance methods, reducing cleaning actions and costs, and retarding surface contamination. In this process, a chemical reaction is initiated when a semiconductor photocatalyst is irradiated by light with an energy that matches or exceeds the band gap energy of the semiconductor, resulting in excited electron-hole pairs formation, that can be applied to the degradation of an organic compound (Hoffmann et al., 1995). Commercial photocatalytic paints contain TiO<sub>2</sub> (anatase) as catalyst, which is activated by photons in the UV-A range for both the oxidation of organic substances and the inactivation of bacteria and viruses. The main applications of these paints are focused on exterior facades, which, via the photocatalytic processes, are maintained clean from organic pollutants and from the growth of microorganisms and fungi (Caballero et al., 2010; Markowska-Szczupak et al., 2010).

The present study is focused on the photocatalytic self-cleaning properties of an innovative paint containing a lanthanum ferrite. LaFeO<sub>3</sub>-based materials have found applications in essential components, such as cathodes in solid oxide fuel cells (Zurlo et al., 2014; Natali Sora et al., 2015), magnetic and electrode materials (Pena and Fierro 2001), chemical sensors (Cavaliere et al., 2012; Tulliani et al., 2015) and catalysts (Tanaka et al., 2005). Moreover, LaFeO<sub>3</sub> was proposed as visible-light photocatalyst in 2007 (Li et al., 2007), although the first detailed study on the photocatalytic degradation of organic compounds was reported by Su et al. (Su et al., 2010), who observed an excellent photocatalytic performance in Rhodamine B degradation in aqueous solution. Successive studies performed using nanostructured LaFeO<sub>3</sub> with different morphologies (Thirumalairajan et al., 2013) confirmed this capability for visible-light degradation of Rhodamine B. Fenton-like reaction could enhance the photocatalytic degradation of Rhodamine B through a synergistic effect (Peng et al., 2016). Little is known about the photocatalytic efficiency of LaFeO<sub>3</sub> under visible-light for the degradation of molecules other than the organic dyes. Recently, it has been reported that LaFeO<sub>3</sub> displayed photocatalytic activity for the degradation of ciprofloxacin (90 %) and ibuprofen (40 %) in water after 5 h visible-light irradiation (Natali Sora and Fumagalli, 2016).

The main components of a water-based photocatalytic paint for outdoor surfaces of buildings are: pigments, mineral fillers, binder, and, of course, water. Minor additives are also present, such as dispersing agent,

wetting agent, anti-foaming agent, rheological agent, thickener, coalescence agent and photocatalyst. Under irradiation the photocatalyst could photooxidise the polymer binder, and as a consequence loss of catalyst particles (photochalking) (Baudys et al., 2015) could take place. To overcome this problem, in this study a paint was used, in which only a small part of the inorganic silicate binder was substituted with an organic binder. In view of the above consideration, investigations were undertaken on paint samples exposed to accelerated ageing tests using a climatic chamber, which simulated weathering agents: UV-A radiation, rainwater and conspicuous temperature and humidity variations. Samples were subsequently tainted by an azo-dye (Procion Red PX-4B), and the color degradation of the taint onto the solid phase was followed by UV-Vis diffuse reflectance spectroscopy (DRS). The relative durability and self-cleaning properties of paints containing  $\text{LaFeO}_3$  were compared to those without catalyst.

## 2. Experimental

### 2.1 Samples preparation and characterization

Lanthanum ferrite  $\text{LaFeO}_3$  was obtained by the citrate auto-combustion method (Caronna et al., 2009). The photocatalytic paint (LF) was prepared by mixing  $\text{LaFeO}_3$  (1 wt%) to a commercial water-based paint. The decision to add only 1 wt% of catalyst was due to the fact that the percentages of the components of the two paints were maintained very similar and in economic terms such amount did not impact much on the price of paint. The paint (P) contained potassium silicate ( $\text{SiO}_2/\text{K}_2\text{O}$ ) as inorganic binder, and, due to technical requirements to use, styrene-acrylic resin (5 wt%). Moreover, other main crystalline components were quartz ( $\text{SiO}_2$ ) and calcite ( $\text{CaCO}_3$ ) as mineral fillers, and rutile ( $\text{TiO}_2$ ) as white pigment. The phase composition of both paints was checked by using X-Rays Diffraction (XRD). The color of the paint with LF was magnolia (a pale pink-orange tone), while the original paint was white.

Two coats of paint were applied to fibre cement plates of area  $6.0 \times 7.5 \text{ cm}^2$ , using a brush. Half of the samples were coated with the reference paint, while the other half with the photocatalytic paint. The edge of the plates was sealed with silicone to prevent the ingress of water, which would have caused swelling of the specimens through the weathering tests, or led to unwanted cracks in the support of the paint during the ice phase. Scanning electron microscopy (SEM) measurements were performed by a TM3030 (HITACHI) tabletop microscopy instrument. FTIR spectroscopy was carried out with a Thermo Scientific Nicolet iS10 equipped with a KBr beam splitter and a DTGS detector. The spectra were collected in the range  $400 - 4000 \text{ cm}^{-1}$  at a resolution of  $4 \text{ cm}^{-1}$ , accumulating 50 scans.

### 2.2 Weathering tests

Some control samples were kept in a dry and dark environment, while the rest were introduced into a laboratory weathering chamber programmed to subject the specimens to adverse environmental conditions (Figure 1). Two sub-cycles were employed; one to simulate rain, freezing, dry heat and humid heat, the second to carry out irradiation using a high pressure Hg lamp ( $125 \text{ W}$ ,  $\lambda_{\text{max}} = 365 \text{ nm}$ ). In Table 1 the experimental conditions associated with each phase are listed. Three specimens of each type (LF and P) were extracted after 10 and 30 aging cycles and twelve after 50 cycles, corresponding to 62 h, 185 h and 308 h of weathering tests, respectively. All specimens were subsequently analysed by UV-Vis diffuse reflectance spectrometry.

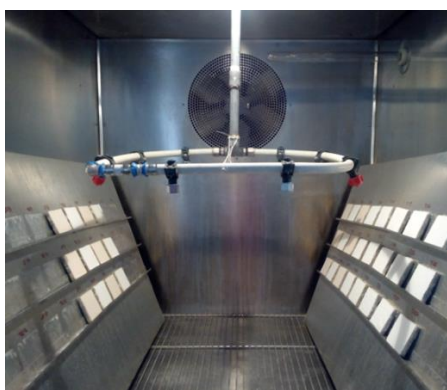


Figure 1: Weathering chamber with samples before starting the last 20 cycles.

Table 1: Experimental conditions of the weathering cycles

Sub-cycle A					
n°	Phase	T <sub>air</sub> [°C]	T <sub>water</sub> [°C]	RH [%]	Duration [min.]
1	Rain	20	15-20	...	60
2	Ice	-20	...	...	90
3	Humid heat	55	...	95	60
4	Dry heat without UV	70	...	40	80

## Sub-cycle B

n°	Phase	T <sub>air</sub> [°C]	T <sub>water</sub> [°C]	RH [%]	Duration [min.]
1	UV Radiation	30	...	40	80

## 2.3 Photocatalytic self-cleaning tests

For the evaluation of the photocatalytic self-cleaning properties, the color degradation of an azo-dye (Procion Red PX-4B, (Dystar, Italy)) onto the paint surface on the plates was monitored after regular intervals of light irradiation. LF is a semiconductor with band gap energy in the range of 2.5-2.6 eV (Parrino et al. 2016, Natali Sora et al. 2013), thus the photocatalytic color degradation reaction was carried out in a photoreactor (Multirays) equipped with 10 lamps (8 W, Daylight) emitting in the visible region. The specimens were placed in an ad-hoc prepared support that rotated about a central axis in order to ensure even exposure to radiation. The dye solution was prepared in a 90:10 (v:v) mixture of acetone and water. The dye concentration was 0.4 g/L. The specimens were tainted by dropping a fixed amount of the dye solution onto the paint surface, then they were left 48 h under dark to allow a complete evaporation of the solvents before starting the self-cleaning tests. Table 2 summarizes the experimental conditions of the samples tested for self-cleaning properties.

Table 2: Experimental conditions of the samples tested for self-cleaning properties. Weathered samples are labeled by W.

Reference samples	Weathering cycles	Vis-light irradiation (h)	Photocatalytic samples	LF (wt%)	Weathering cycles	Vis-light irradiation (h)
P	0	0	LF	1	0	0
P1	0	120	LF1	1	0	120
P2	0	240	LF2	1	0	240
P3	0	360	LF3	1	0	360
PW	50	0	LFW	1	50	0
PW1	50	120	LFW1	1	50	120
PW2	50	240	LFW2	1	50	240
PW3	50	360	LFW3	1	50	360

The color degradation of the dye on the paint layer was followed in solid phase by diffuse reflectance spectrometry (DRS). The DRS spectra were collected using an ultraviolet-visible (UV-Vis) spectrophotometer (Jasco V-650), equipped with a 60 mm integrating sphere. The Kubelka-Munk (K-M) equations were used to transform the reflectance data into the absorption data (Kubelka and Munk, 1931). Diffuse reflectance  $R$  of the sample was related to its absorption  $K$  and scattering characteristics  $S$  as Eq(1):

$$\left(\frac{K}{S}\right) = \frac{(1-R_\infty)^2}{2R_\infty} \quad (1)$$

The dye photodegradation percentage of the Procion Red PX-4B azo-dye was calculated from the absorption intensity data at the  $\lambda_{\max} = 551$  nm for all the LF and LFW series, and  $\lambda_{\max} = 548$  nm for all the P and PW series using the Eq(2):

$$\text{Dye Photodegradation (\%)} = \left(1 - \frac{D_t}{D_0}\right) \times 100 \quad (2)$$

where  $D_0 = \left(\frac{K}{S}\right)_0 - \left(\frac{K}{S}\right)_p$ , and  $\left(\frac{K}{S}\right)_p$  was the K-M value of the untainted paint, while  $\left(\frac{K}{S}\right)_0$  was the K-M value of the dye before exposure to the visible-light irradiation. Correspondingly,  $D_t = \left(\frac{K}{S}\right)_t - \left(\frac{K}{S}\right)_p$  where  $\left(\frac{K}{S}\right)_t$  was the K-M

value after irradiation to  $t = 120, 240$  and  $360$  h. For each sample the measurements were performed on two different tainted regions.

### 3. Results and Discussion

#### 3.1 Microstructural characterization of paint coatings

The paint surface on the specimens (LFW and PW series) subjected to the first 30 cycles showed a small bulging. The damage slightly increased with further weathering cycles (Figure 2), due to the fact that the content of resin in the paint film was only 5 wt%, and as a consequence the film exhibited a permeability to water vapour. The water vapour condensed under the film, but in the weathering chamber during the dry heat phase it evaporated generating bubbles. The results are in agreement with a recent study, which reported how weathering may influence the durability of silicate-based paint (Baudys et al., 2017).

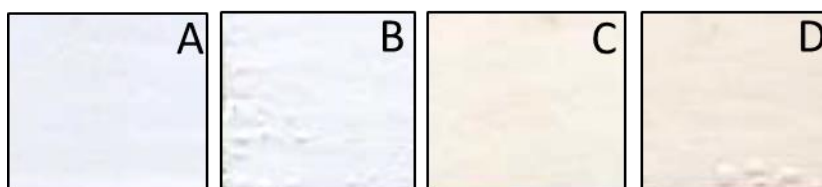


Figure 2: Images of A) unweathered P reference paint; B) 50 cycles weathered PW reference paint; C) unweathered LF photocatalytic paint; D) 50 cycles weathered LFW photocatalytic paint.

SEM analysis evidenced that the surface of the weathered samples (LFW and PW) showed slight pitting compared to the unweathered ones. The presence of the  $\text{SiO}_2$  phase was evidenced in two morphologies: a porous structure due to nanocrystalline silicate binder and large crystalline particles. Moreover, backscattered electron images (BSE) were used for rapid discrimination of phases in the samples. The distribution of "brighter" BSE intensity (correlated with the  $\text{LaFeO}_3$  photocatalyst) were very similar in LF and LFW series indicating negligible loss of catalyst particles in the weathered paints. On the contrary, Si-map of LFW was poorer of the Si element respect to LF. The weathering treatments increased the roughness of the surface of both paints, which is supposed to be due to some loss of the silicate.

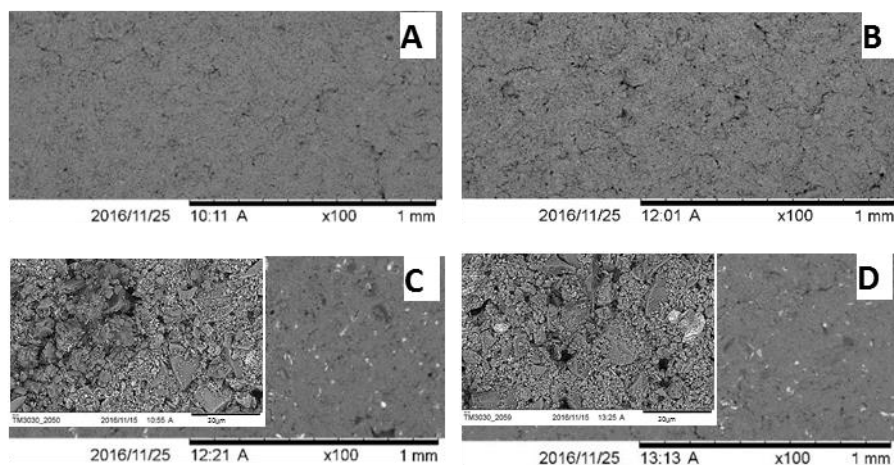


Figure 3: SEM micrographs of A) unweathered P reference paint; B) 50 cycles weathered PW reference paint; C) unweathered LF photocatalytic paint; D) 50 cycles weathered LFW photocatalytic paint.

The FTIR spectra of LF and LFW were similar but with some exceptions: the broad peak at ca.  $1082\text{ cm}^{-1}$  corresponding to the asymmetric stretching of Si-O-Si overlapping the Si-O-K band vibrations (data not shown here), and the broad carbonate multiple peak at  $1400\text{-}1520\text{ cm}^{-1}$ . The silicate peak was stronger for unweathered LF paint, in agreement with the fact that the LFW coating has lost a small fraction of surface silicate. Also the carbonate peak slightly stronger for the LF unweathered sample. The weak peak at  $1736\text{ cm}^{-1}$  was assigned to the carbonyl (C=O) stretching vibration. The latter peak which is characteristic of the

styrene-modified acrylic resin (Germinario et al., 2016) was identical in both (LF and LFW) spectra indicating that the nature of the resin was not modified by the weathering tests.

### 3.2 Photocatalytic self-cleaning tests

The self-cleaning tests were done in parallel using reference and photocatalytic paints, in order to validate the reproducibility of LF catalytic behavior. As shown in Figure 4A the dye degradation percentage of Procion Red PX-4B using non weathered paint (LF) under visible-light irradiation (360 h) was 78 %. The discoloration percentage of samples LF1, LF2 and LF3 were always higher compared to the reference P1, P2 and P3 samples, the difference in degradation percentage was constant at longer visible-light irradiation time. A similar behavior was found with weathered paint films. After 360 h irradiation the dye with LFW3 paint displayed a dye degradation percentage of 67 % (Figure 4B). Also in this case the dye discoloration of samples LFW1, LFW2 and LFW3 was always higher compared to the reference PW1, PW2 and PW3 samples, and the difference in degradation percentage was unchanging with longer irradiation time. Photocatalytic tests performed in aqueous solution with powder slurries as catalyst guarantee a continuous contact between the target molecules and the nanoparticles of the catalyst. In our case, the photodegradation experiments were carried out using LF in the solid paint matrix. This experimental configuration did not guarantee high accessibility to the catalyst by the dye molecules. Moreover, in this case the amount of catalyst was small (1 wt%), therefore contribution arising from direct photolysis of the dye was the most important after long irradiation time (360 h). The difference in the percentage of degradation between P and LF specimens was, in our opinion, due to the presence of the photocatalyst.

The partial loss of nanocrystalline silicate and the consequent surface roughness modification, induced by the exposure of silicate binder to extreme experimental conditions in the climatic chamber may cause the decrease of the self-cleaning performances in the weathered samples. In fact, the slight increase in the superficial amount of acrylic resin which didn't present the hydrophilic and porous nature of the potassium silicate prevented a homogeneous distribution of the dye solution onto the paint films. Moreover, as described in section 3.1 BSE images indicated not significant loss of catalyst particles in the weathered paints. The lowering of self-cleaning efficiency is not due to the loss of catalyst, but to a microstructural variation of the paint surface.

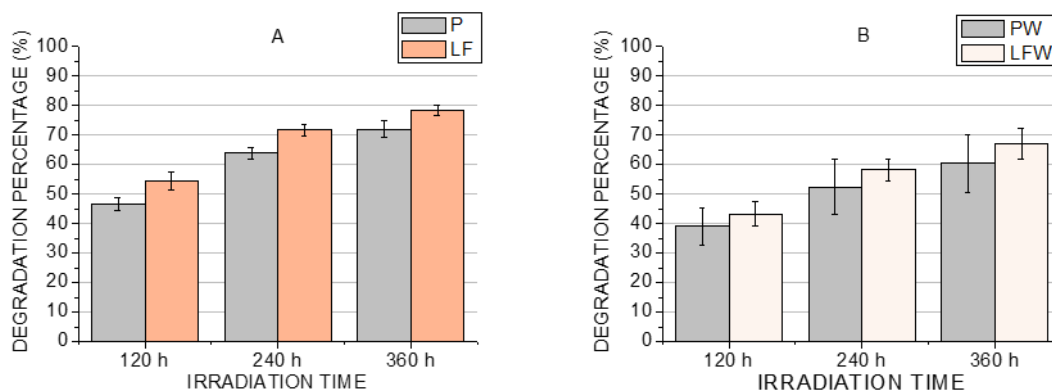


Figure 4: Photocatalytic dye degradation percentage of Procion Red PX-4B after 120, 240, 360 h visible-light irradiation in: A) unweathered samples; B) weathered samples.

## 4. Conclusions

Water-based silicate-acrylic paint (reference paint) with the addition of 1 wt% of  $\text{LaFeO}_3$  catalyst was tested for color degradation under visible-light irradiation of the Procion Red PX-4B azo-dye. The addition of 1 wt% of catalyst in economic terms did not impact much on the price of paint. Both photocatalytic and reference paints, exposed to accelerated weathering tests, showed a decrease in self-cleaning properties due, in our opinion, to some loss of the silicate induced by the treatments in the climatic chamber. The color degradation of the photocatalytic paint was higher than that of the corresponding reference paint, both in weathered and unweathered conditions. The difference in degradation percentage was constant up to 360 h of exposure to visible-light.

## Acknowledgments

The authors thank prof. Bruno Daniotti (Polytechnic of Milano) for helpful discussions and dr. Claudia Tiraboschi for collaboration in the use of climatic chamber. We are indebted with University of Las Palmas prof. Francisco Javier Araña Mesa and prof. Oscar Manuel González Díaz for the SEM and FTIR measurements.

## References

- Baudys M., Krýsa J., Zlámál M., Mills A., 2015, Weathering tests of photocatalytic facade paints containing ZnO and TiO<sub>2</sub>, *Chem. Eng. J.* 261, 83-87
- Baudys M., Krýsa J., Mills A., 2017, Smart inks as photocatalytic activity indicators of self-cleaning paints, *Catal. Today* 280, 8-13
- Caballero L., Whitehead K.A., Allen N.S., Verran J., 2010, Photoinactivation of Escherichia Coli on acrylic paint formulations using fluorescent light, *Dyes and Pigments* 86, 56-62
- Caronna T., Fontana F., Natali Sora I., Pelosato R., 2009, Chemical synthesis and structural characterization of the substitution compound LaFe<sub>1-x</sub>Cu<sub>x</sub>O<sub>3</sub> (x = 0-0.40), *Mat. Chem. Phys.* 116, 645-648
- Cavaliere A., Caronna T., Natali Sora I., Tulliani J.M., 2012, Electrical characterization of room temperature humidity sensors in La<sub>0.8</sub>Sr<sub>0.2</sub>Fe<sub>1-x</sub>Cu<sub>x</sub>O<sub>3</sub> (x = 0, 0.05, 0.10), *Ceram. Int.* 38, 2865-2872
- Germinario G., van der Werff I.D., Sabbatini L., 2016, Chemical characterization of spray paints by multi-analytical (Py/GC, FTIR, m-Raman) approach, *Microchem. J.* 124, 929-939
- Hoffmann M., Martin S.T.W., Bahnemann D.W., 1995, Environmental applications of semiconductor photocatalysis, *Chem. Rev.* 95, 69-96
- Kubelka P., Munk F., 1931, Ein Beitrag zur Optik von Farbanstrichen, *Z. für Tech. Phys.* 12, 593-601
- Li S., Jing L., Fu W., Yang L., Xin B., Fu H., 2007, Photoinduced charge property of nanosized perovskite-type LaFeO<sub>3</sub> and its relationships with photocatalytic activity under visible irradiation, *Mater. Res. Bull.* 42, 203-212
- Markowska-Szczupak A., Ulfing K., Grzmil B., Morawski A.W., 2010, A preliminary study on antifungal effect of TiO<sub>2</sub>-based paints in natural indoor light, *Polish J. Chem. Technol.* 12, 53-57
- Natali Sora I., Fontana F., Passalacqua R., Ampelli C., Perathoner S., Centi G., Parrino F., Palmisano L., 2013, Photoelectrochemical properties of doped lanthanum orthoferrites, *Electrochimica Acta* 109, 710-715
- Natali Sora I., Felice V., Zurlo F., Licocchia S., Di Bartolomeo E., 2015, Characterization of Tantalum Doped Lanthanum Strontium Ferrite as Cathode Materials for Solid Oxide Fuel Cells, *J. Alloys and Compounds* 648, 154-159
- Natali Sora I., Fumagalli D., 2016, Fast photocatalytic degradation of pharmaceutical micropollutants and ecotoxicological effects, *Environ. Sci. Pollut. Res.* DOI 10.1007/s11356-016-7640-y
- Parrino F., García-López E., Marci G., Palmisano L., Felice V., Natali Sora I., Armelao L., 2016, Cu-substituted lanthanum ferrite perovskites: preparation, characterization and photocatalytic activity in gas-solid regime under simulated solar light irradiation, *J. Alloys Comp.* 682, 686-694
- Peña M.A., Fierro J.L.G., 2001, Chemical structures and performance of perovskite oxides, *Chem. Rev.* 101, 1981-2017
- Peng K., Fu L., Yang H., Ouyang J., 2016, Perovskite LaFeO<sub>3</sub>/montmorillonite nanocomposites: Synthesis, interface characteristics and enhanced photocatalytic activity, *Scientific Reports* 6, 19723
- Su H., Jing L., Shi K., Yao C., Fu H., 2010, Synthesis of large surface area LaFeO<sub>3</sub> nanoparticles by SBA-16 template method as high active visible photocatalysts, *J. Nanopart. Res.* 12, 967-974
- Tanaka H., 2005, An intelligent catalyst: the self-regenerative palladium-perovskite catalyst for automotive emissions control, *Catal. Surv. Asia* 9, 63-74
- Thirumalairajan S., Girija K., Hebalkar N.Y., Mangalaraj D., Viswanathan C., Ponpandian N., 2013, Shape evolution of perovskite LaFeO<sub>3</sub> nanostructures: A systematic investigation of growth mechanism, properties and morphology dependent photocatalytic activities, *RSC Advances* 3, 7549-7561
- Tulliani J-M., Natile M.M., Tortora L., Natali Sora I., 2015, Ageing of lanthanum strontium copper orthoferrite powders for sensing layers, *Chem. Eng. Transactions* 43, 1807-1812
- Zurlo F., Di Bartolomeo E., D'Epifanio A., Felice V., Natali Sora I., Tortora L., Licocchia S., 2014, La<sub>0.8</sub>Sr<sub>0.2</sub>Fe<sub>0.8</sub>Cu<sub>0.2</sub>O<sub>3-δ</sub> as "cobalt free" cathode for La<sub>0.8</sub>Sr<sub>0.2</sub>Ga<sub>0.8</sub>Mg<sub>0.2</sub>O<sub>3-δ</sub> electrolyte, *J. Power Sources* 271, 187-194